Charge-Based Chemical Sensors: A Neuromorphic Approach With Chemoreceptive Neuron MOS (CνMOS) Transistors

Nick Yu-Min Shen, *Student Member, IEEE*, Zengtao Liu, Chungho Lee, Bradley A. Minch, *Member, IEEE*, and Edwin Chih-Chuan Kan, *Member, IEEE*

***Abstract*—A novel chemoreceptive neuron MOS (CνMOS) transistor with an extended floating-gate structure has been designed with several individual features that significantly facilitate system integration of chemical sensing. We have fabricated CνMOS transistors with generic molecular receptive areas and have characterized them with various fluids. We use an insulating polymer layer to provide physical and electrical isolation for sample fluid delivery. Experimental results from these devices have demonstrated both high sensitivity via current differentiation and large dynamic range from threshold voltage shifts in sensing both polar and electrolytic liquids. We have established electrochemical models for both steady-state and transient analyses. Our preliminary measurement results have confirmed the basic design and operations of these devices, which show potential for developing silicon olfactory and gustatory units that are fully compatible with current CMOS technology.**

***Index Terms*—Chemical sensors, floating-gate devices, microfluidic channels, neuromorphic sensing, neuron MOS transistors.**

I. Introduction

DESIGN considerations for microsensors include high sensitivity, high selectivity, large dynamic range, simple calibration/reset protocols, field reconfigurability, reproducibility, stability, low power consumption, and low manufacturing cost. Efforts have been made along this direction for over thirty years with various fruitful approaches, including field-effect transistors (FET)-based sensors, chemiresistors, chemicapacitors, microelectrode, microcalorimeter, surface acoustic wave (SAW) devices, and chemomechanical sensors [1]–[21].

In developing an autonomous system for monitoring chemical and molecular substances, devices integrated with CMOS transistors are of special interests, not only because existing CMOS technology can provide accurate control circuitry, but also because affordable mass production is readily available. Our chemoreceptive neuron MOS transistor is based upon the combination of FET-based sensors [1]–[3], chemicapacitors [5], and neuron MOS (νMOS) transistors [22], with a novel extended floating-gate structure for molecular and chemical sensing, and it can be fabricated by a simple post-processing of conventional CMOS integrated circuits.

The concept of adapting floating-gate structures for sensing purpose has been explored in the past. For example, the extended floating-gate structure in [6] is used as a signal line with one end coated with the chemically sensitive membrane, and the polysilicon layer on top of the floating gate (FG) serves as a guard/shield for the signal line. The FG in [7] and [8] is covered with Si_3N_4, which is adapted as the sensing layer. Compared with those contributions, the structure proposed in this paper uses the extended FG with the sensing signal coming in capacitively. Furthermore, we can configure the total amount of charge from electron injection onto the FG to further enhance the signature analysis and the potential fluidic actuation.

II. Device Design and Fabrication With Modular Isolation Scheme

Fig. 1 illustrates the device profile and the circuit symbol of a chemoreceptive neuron MOS (CνMOS) transistor. The MOS area has very similar fabrication requirements to those at commercial Flash EEPROM [23], in which the FG is primarily adapted for nonvolatile storage. Shibata and Ohmi [22] broadened the function of floating-gate devices by introducing the νMOS concept. The characteristic feature of the νMOS transistor is that such devices can be constructed with any number of control-gate electrodes, which couple into the FG capacitively. The floating-gate voltage is established through charge sharing or capacitive voltage division, as a weighted sum of the voltages that are applied to the control gates (CGs). The weight on each CG is directly proportional to the capacitance of that CG and is normalized by the total capacitance of the FG. This basic operation principle is similar to that implemented by neurons [22] and synapses [24], whence the "neuron" in the name.

Based on the νMOS concept, some control-gate electrodes can be further designed to proper dimensions in order to capture the input information provided by the fluidic contact through electrostatic coupling. As a demonstration, we fabricated the silicon chip through a commercial foundry (i.e., MOSIS AMIS 1.5-μm). The n-channel MOSFET containing the source and drain structure has a W/L ratio of 2.5 and the thicknesses of the gate oxide and the inter-poly oxide are approximately 30 and 58 nm, respectively. Although the device dimension had not been optimized for operations, the basic design demonstrated the compatibility of our CνMOS transistors with existing CMOS technology.

Manuscript received April 10, 2003; revised July 2, 2003. This project is supported in part by the National Science Foundation through Nanoscale Exploratory Research Grant ECS-0210743, and by the Environmental Protection Agency through National Center for Environmental Research Grant R830902. The review of this paper was arranged by Editor K. Najafi.

The authors are with the School of Electrical and Computer Engineering, Cornell University, Ithaca, NY 14853 USA (e-mail: ys69@cornell.edu).

Digital Object Identifier 10.1109/TED.2003.816905

0018-9383/03$17.00 © 2003 IEEE

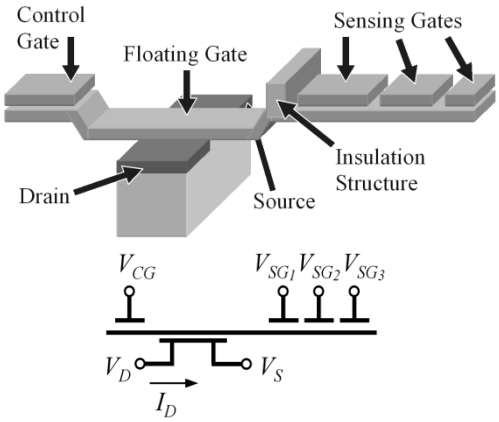

Fig. 1. Illustration of a CνMOS transistor. (a) Three-dimensional rendering of the device structure with potential multiple sensing gates (SGs) (b) Circuit symbols showing one input assigned as a CG and three other inputs as chemoreceptive SGs with applicable chemical coatings.

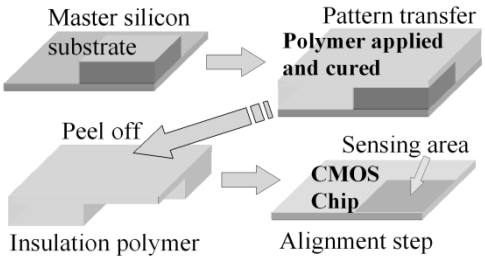

Fig. 2. Illustration of the pattern transfer from the master silicon substrate to the device-encapsulation polymer layer. Sensing area and channel height are defined during the fabrication of the master silicon substrate. The polymer layer is applied and cured on the master silicon substrate, and then peeled off for alignment on the MOS devices.

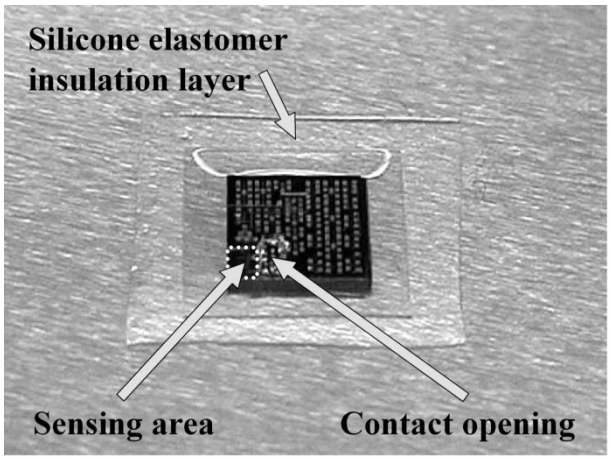

(a)

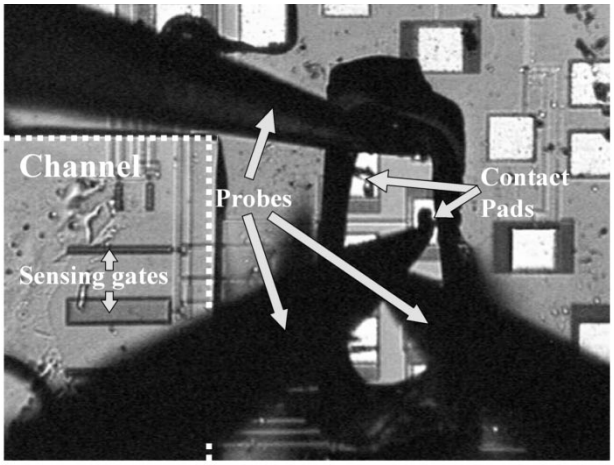

(b)

Fig. 3. (a) Top view of the polymer insulation layer aligned to a CMOS chip resting on an aluminum tray with contact openings, which are made by the addition of Epoxy 907 on top of the master silicon substrate during pattern transfer; (b) Close-up view of the channel and device area with the illustration of probing through contact openings. Fluids are delivered through the microfluidic channels overlapping the extended FG of the test EEPROM device and are confined in the sensing areas by the insulation polymer.

To prepare a CνMOS transistor for testing, an extra master silicon substrate is adapted to define the microfluidic channel area, as illustrated in Fig. 2. The master silicon substrate made with the deep reactive ion etching (DRIE) method also defines the channel height, which is about 150 μm in our case. The pattern is then transferred to the insulation polymer layer formed by mixing 20 parts of silicone elastomer base with one part of curing agent (Sylgard 184, Dow Corning). The encapsulated microfluidic channels for control fluid delivery are shaped by bonding the patterned polymer layer on top of the 4.6 mm $\times$ 4.7 mm CMOS chip, as shown in Fig. 3(a). Fig. 3(b) provides a closer view of the sensing areas and the contact pads for probing purposes. The sensing gates are exposed by an oxide etch and are aligned with the polymer microfluidic channels, which confine the fluid as well as keep the devices physically and electrically isolated. Two different SG areas are adapted to facilitate comparison. Device 1 has a sensing area of 4.8 μm $\times$ 356.8 μm and device 2 of 76.8 μm $\times$ 356.8 μm.

The modular structure of this isolation scheme provides flexibility in the design and composition of various chemoreceptive coatings for higher selectivity, while keeping CMOS devices optimized for high sensitivity and large dynamic range. The capacitive coupling from the fluidic area will influence the channel current through the high internal gain stemming from the transconductance of the MOS transistor. Given that the MOS area is well protected physically, we can aggressively design the transistor for appropriate transconductance and subthreshold slope without contamination and oxide reliability concerns.

III. Principle of Operations and Measurement Results

At the proof-of-concept stage, we opted to use polysilicon directly as the chemoreceptive sensing surface to interact with various sample fluids. The sensing polysilicon is electrically isolated from the extended floating-gate polysilicon by an inter-poly oxide of about 58 nm. The measurement begins with a recording of the original current–voltage (I–V) characteristics of the EEPROM device both with and without the bonded insulation polymer layer on top of the CMOS chip. Various sample fluids are then delivered to the encapsulated microfluidic channels individually on different chips. The fluid interacts with the polysilicon surface on the SG through the formation of electrical double layers at the solid/liquid interface [25]. The capacitive load and static charges introduced onto the FG will cause specific changes in both subthreshold slopes and threshold voltages. The total nonvolatile charges on the FG will

further influence the interaction with the fluid at the interface. The channel current from the control-gate voltage swing then serves as a signature for the fluid and its solute contents. High sensitivity is derived from the high transconductance gain of the MOS transistor and a large dynamic range from the large control-gate voltage ramp achieved concurrently.

After measuring the full-swing *I–V* curves for each type of sample fluid in the encapsulated channel, electrons are tunneling onto and off of the FG of the CνMOS device by a fixed bias at the CG, 30 V for tunneling in and -30 V for tunneling out. The *I–V* characteristics of various sample fluids are separately recorded after the electron tunneling operations. The drain voltage is biased at 0.5 V for all the measurements to prevent hot-carrier injection and to ensure the device is in the saturation region during subthreshold operation. The measurement results are listed with notations in Tables I and II, with selected figures shown (see Figs. 4–7).

In Table I, the threshold voltage shifts ΔV_t are obtained sequentially in various operations, with each preceding V_t as the reference for extraction. Labels d1 and d2 denote devices 1 and 2 with different fluid-interacting areas (1 : 16) of the SGs. Letters "i" and "o" correspond to electron tunneling in and out of the FGs of the test devices when the microfluidic channels are filled with various fluids. Control samples have no fluid in the microfluidic channels while performing electron tunneling. For the saturated saline water tests, the difference in voltage shift direction (boldfaced values) indicates charge redistribution at the solid/liquid interface.

In Table II, a smaller S indicates a more rapid change in the *I–V* curves, since the subthreshold parameter S (mV/decade current) expresses the change of $\log_{10}(I_D)$ with respect to the control-gate voltage sweep. Labels of d1, d2, "i," and "o" follow the same notation as in Table I. The label "c" denotes measurements before fluid delivery, "m" denotes right after fluid application, and "t" represents measurements in a long time interval, from 18 hours to 15 days, after the excessive charge on the FG leak away and the applied fluids dry up from the microfluidic channels. The changes in subthreshold slopes for device 2 after electron tunneling operations for the saturated saline water tests again indicate the possibility of the charge redistribution at the solid/liquid interface.

We also monitor the *I–V* relationship at the transient mode on our CνMOS transistors with sample fluids in the microfluidic channels. An ac signal with 5 V amplitude is applied at the CG, with the frequency ranging from 1 Hz to 1 MHz. The monitored channel current is amplified and converted to the voltage signal through a transimpedance amplifier with the sensitivity set at 50 μA/V, and the output voltage is then examined on an oscilloscope. Selected transient-response measurement results are shown in Figs. 8–12.

IV. Steady-State and Transient Analyses

For the steady-state analysis, the subthreshold current $I_{D\mathrm{sub}}$ and threshold voltage V_t for a multiple-input floating-gate MOS transistor [26] can be written as

$$I_{D\mathrm{sub}} = I_0 e^{\kappa V_{\mathrm{FG}}/U_T}(e^{-V_S/U_T} - e^{-V_D/U_T}) \tag{1}$$

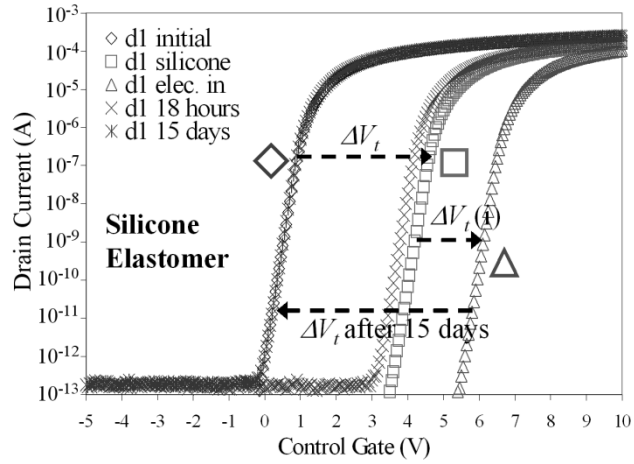

Fig. 4. *I–V* characteristics are recorded when silicone elastomer contacts the exposed SG by pressure. Notations follow those in Tables I and II. The almost-unaltered subthreshold slope implies the open-circuit condition at the FG.

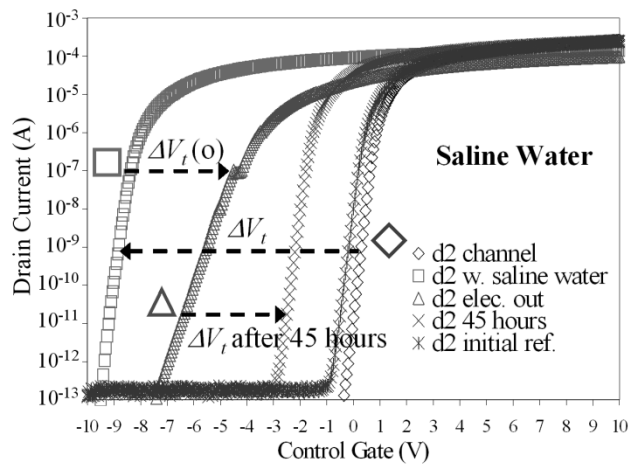

Fig. 5. Saturated saline water is first delivered to the channel, and then the electrons are tunneling out of the FG. Notice the apparent shift of the threshold voltage.

$$V_t = V_{t0} - \frac{Q}{C_T} - \frac{C_{gs}}{C_T} V_S - \frac{C_{\mathrm{gd}}}{C_T} V_D. \tag{2}$$

The body coefficient κ is defined as $\kappa = C_{\mathrm{ox}}/(C_{\mathrm{ox}} + C_{\mathrm{dep}})$, and the thermal voltage is $U_T = kT/q$, where k is the Boltzmann constant, T the temperature, and q the elementary charge. V_S and V_D are the voltages at the source and drain. The floating-gate voltage V_{FG} can be expressed as a weighted sum through charge sharing or capacitive voltage division, including those from all CGs and SGs labeled from 1 to N

$$V_{\mathrm{FG}} = \frac{Q}{C_T} + \frac{C_{gs}}{C_T} V_S + \frac{C_{\mathrm{gd}}}{C_T} V_D + \sum_{j=1}^{N} \frac{C_j}{C_T} V_j \tag{3}$$

where the total capacitance C_T can be written as

$$C_T = (C_{\mathrm{ox}} // C_{\mathrm{dep}}) + C_b + C_{gs} + C_{\mathrm{gd}} + \sum_{j=1}^{N} C_j. \tag{4}$$

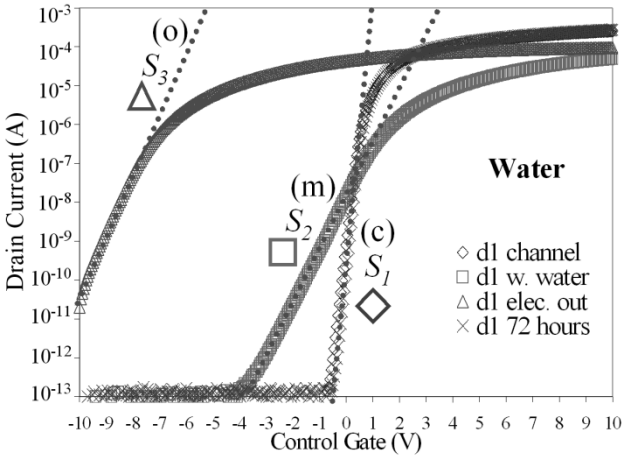

Fig. 6. Combination of the threshold voltage shift ΔV_t and the subthreshold slope S provides the *I–V* signatures of liquids on chemical coatings, water on polysilicon in this case.

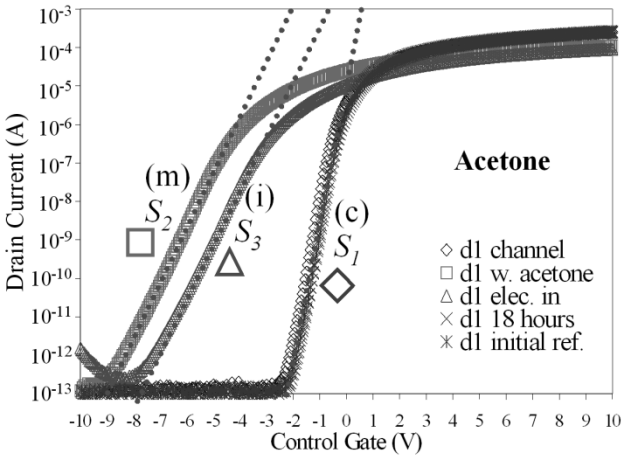

Fig. 7. The different *I–V* behavior of water and acetone on polysilicon primarily stems from the smaller ionic strength of acetone. The initial drop of the drain current in the electron injection curve indicates the generation-recombination condition in the channel. The R-G phenomenon lasts a few seconds after the light source is removed.

TABLE I
THRESHOLD VOLTAGE SHIFTS ΔV_t OF THE CνMOS TRANSISTORS

ΔV_t (V)	electron tunneling in				electron tunneling out			
	d1	d1i	d2	d2i	d1	d1o	d2	d2o
water	1.5	3.0	2.5	6.4	1.2	-8.1	1.9	-2.2
acetone	-3.2	1.1	3.8	3.8	-3.1	-4.9	2.8	-7.0
saline	-2.5	**-3.2**	-8.0	10.9	-6.9	-1.5	-9.0	**4.4**
silicone	3.7	1.8	2.6	3.0	1.8	-2.8	1.7	-4.7
control	0.0	4.2	0.0	4.9	0.0	-6.0	0.0	-5.7

Q is the total static charge stored on the FG. C_j and V_j are the capacitance and voltage at the jth-input gate. The capacitances $C_{\rm ox}$, $C_{\rm dep}$, C_{gs}, and $C_{\rm gd}$ follow the same definitions as in conventional MOS transistors [27]. $C_{\rm ox}$ is the gate oxide capacitance, and $C_{\rm dep}$ is the depletion-layer capacitance in the silicon substrate under the gate area. C_{gs} and $C_{\rm gd}$ are the capacitances from the FG to the overlapped source and drain region respectively. C_b is the capacitance from the FG to the bulk [26]. The threshold voltage shift ΔV_t is highly sensitive to the change of Q since V_D is set at a small value. Q is estimated to be only around pCoul level to create several volts of the threshold voltage shift.

The subthreshold slope S reflects the variation of $\log_{10}(I_{D\rm sub})$ with respect to the control-gate voltage ($V_{\rm CG}$) ramp and can be defined as $S \equiv [\partial(\log_{10} I_{D\rm sub})/\partial V_{\rm CG}]^{-1}$. Derived from (1) and (3), the subthreshold slope can be expressed as a function of the control-gate capacitance $C_{\rm CG}$ and the total capacitance C_T

$$S = \frac{U_T \ln 10}{\kappa}\left(\frac{C_T}{C_{\rm CG}}\right). \tag{5}$$

In the case of silicone elastomer (see Fig. 4), the unchanged subthreshold slope demonstrates an open-circuit condition seen at the extended FG, contributing no additional capacitive load to the FG. For the saturated saline water (see Fig. 5), the excessive positive and negative mobile ions in the solution both accumulate at the solid/liquid interface, and thus leave the charge distribution undisturbed at the extended FG, so the subthreshold slope is almost unaltered before the electron tunneling operation. Notice the changes in subthreshold slopes and threshold voltages for saturated saline water after the electron tunneling is performed. This implies the charge redistribution at the solid/liquid interface because of the numerous mobile ions in the saturated saline water responding to the charges at the FG. The charge interaction further suggests the feasibility of an actuation scheme, in which the number or distribution of interface charges can be modified in correspondence with the charges tunneled from the CG into the FG. This type of actuation can be utilized in modifying the surface hydrophobicity (e.g., electrowetting [28], [29]), or in electroosmotic [30] and electrophoretic [31] applications.

For water and acetone (see Figs. 6 and 7), the subthreshold slopes change significantly due to the dominant diffuse capacitors in the liquids. According to the Gouy–Chapman–Stern (GCS) model [25], the diffuse capacitance per unit area $C_{\rm dif}$ can be estimated by

$$C_{\rm dif} = \left(\frac{2\varepsilon_r\varepsilon_0 z^2 q^2 n}{kT}\right)^{1/2} \cosh\left(\frac{zq\phi_2}{2kT}\right) \tag{6}$$

where ε_r is the relative permittivity of the solution, ε_0 the permittivity in vacuum, z the magnitude of the charge on the ions, n the concentration of the potential-determining ions [32] in the liquid bulk, and ϕ_2 the potential at the Outer Helmholtz Plane (OHP). The OHP [25] can be envisioned as the closest plane where the solvated ions can approach due to the finite size of those nonspecifically-adsorbed ions. The pH value for DI water is around 5.5 and is around 7 for acetone, and is used to calculate the concentration n.

Table III lists the capacitance values (in pF) extracted from the subthreshold slopes in Table II with corresponding sensing areas, including the calculation of the fringing-field effect [33]. CGs are assumed to have the same areas in capacitance calculation ($C_{\rm CG}$) regardless of fabrication variations, and so are the initial capacitances for SGs ($C_{\rm SG0}$) before the fluid application.

TABLE II
SUBTHRESHOLD SLOPES S OF THE CνMOS DEVICES

Subthreshold S (mV/dec. A)	electron tunneling in								electron tunneling out							
	d1c	d1m	d1i	d1t	d2c	d2m	d2i	d2t	d1c	d1m	d1o	d1t	d2c	d2m	d2o	d2t
water	183	743	803	173	288	1117	1196	173	171	732	677	160	175	1027	960	170
acetone	269	681	723	259	237	847	965	187	249	684	626	254	180	869	843	171
saline	163	260	244	168	181	238	**1014**	210	160	212	198	170	164	183	**483**	190
silicone	172	176	172	167	204	199	196	182	176	177	176	167	247	214	201	180
control	181	NA	184	178	262	NA	248	229	181	NA	170	167	241	NA	195	176

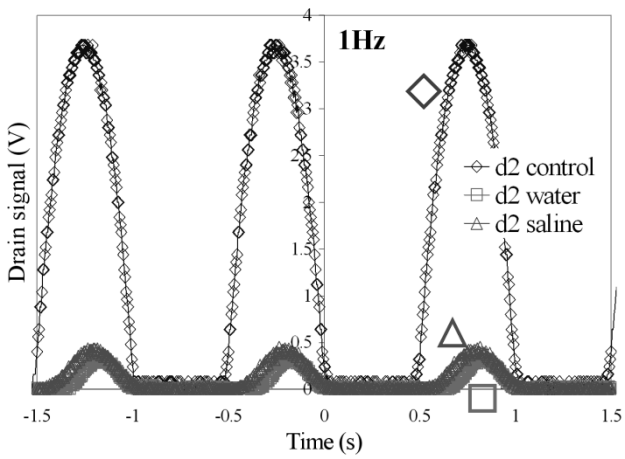

Fig. 8. Channel current responding to a 1 Hz control-gate voltage signal. The smaller amplitude for water and saturated saline water tests results from the smaller offset voltage V_{CG0}. The monitored output voltage is acquired from the amplified channel current signal through a transimpedance amplifier, with the sensitivity set at 50 μA/V.

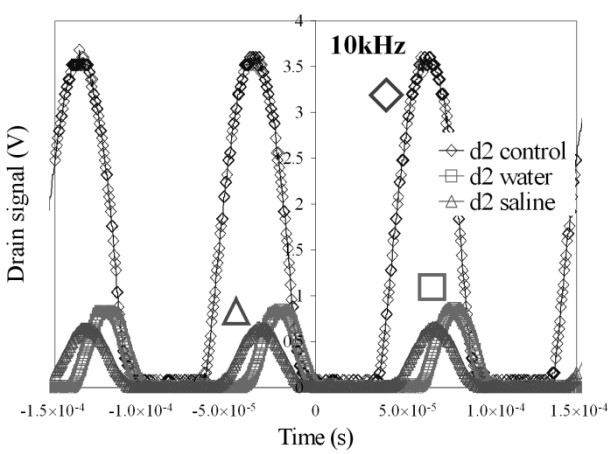

Fig. 9. Transient response with control-gate voltage signal at 10 kHz. The channel signal still manages to have a quasistatic response. The slight increase in channel current for water and saturated saline water measurements might result from the change in Q or C_T or the combination of both factors from the charge variation at the solid/liquid interface.

The oxide thicknesses are estimated as 30 nm, 58 nm, and 1 μm for gate oxide, inter-poly oxide, and field oxide. C_{Tc} and C_{Tm} denote the total capacitances before and after the fluid is delivered to the SG and are extracted according to the subthreshold

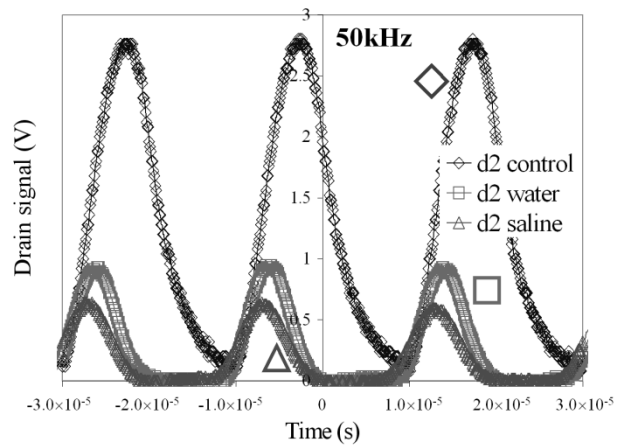

Fig. 10. Control-gate voltage signal has an operational frequency of 50 kHz. The channel current response for the control sample is getting out of the quasistatic region as indicated by the deformation of the waveform.

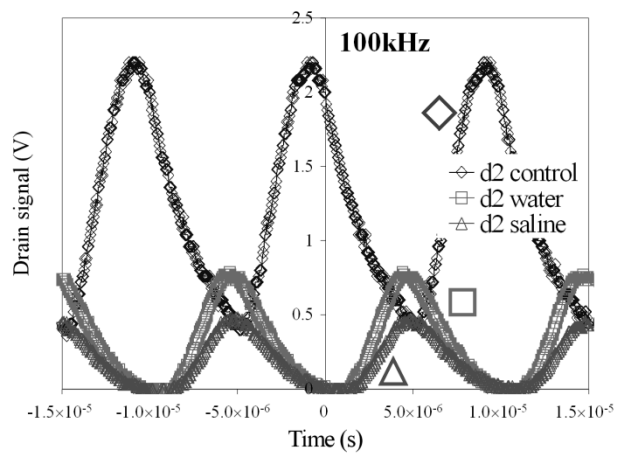

Fig. 11. At 100 kHz, the frequency response begins to leave the quasistatic region in the water sample as well as in the saturated saline water test.

slopes assuming $\kappa = 0.8$. C_{SG} is the capacitance seen at the SG, and can be expressed as $C_{\mathrm{SG}} = (C_{\mathrm{SG0}}//C_{\mathrm{difA}})$, where C_{difA} is the diffuse capacitance with corresponding sensing areas in devices 1 and 2. Adapting (6), the potential ϕ_2 (in mV) at the OHP can be extracted from the diffuse capacitance per unit area C_{dif} in the liquid bulk, and is also listed in Table III.

The values of ϕ_2 usually range from tens to hundreds of millivolts [32], and they indicate both the charge condition at the

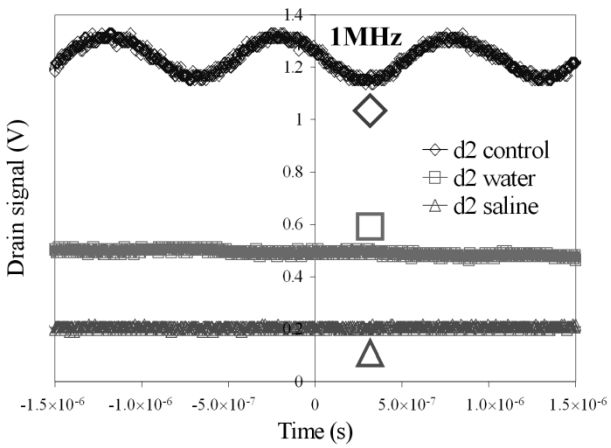

Fig. 12. With frequency at 1 MHz, the control-gate signal is almost seen as a constant input. The floating-gate charge and thus the channel current fails to respond to the input signal at such a high frequency.

solid/liquid interface and the closest distance the solvated ions can reach [25]. Although the relative permittivity of the solution is known to be potential-dependent [34] due to local polarization level, it is assumed to be constant in our extraction of ϕ_2 for the ease of calculation in the conceptual demonstration. According to Table III, the extracted values of ϕ_2 have a discernible difference between water and acetone, and are expected to be characteristic with respect to the fluid interface. Therefore, ϕ_2 can be further exploited in signature analysis or in electroosmotic and electrophoretic actuations [32], although an accurate determination of ϕ_2 is rather difficult.

For the transient analysis, Figs. 8 and 9 represent the quasistatic behavior at frequencies 1 Hz–10 kHz for all three types of measurements, the control devices, the devices with water, and the devices with saturated saline water. The time-varying control-gate voltage $\tilde{v}_{\rm CG}$ can be expressed as

$$\tilde{v}_{\rm CG} = V_{\rm CG0} + V_{\rm CG} \sin \omega t \tag{7}$$

where $V_{\rm CG0}$ is the offset voltage at the CG and ω is the angular frequency of the applied ac signal.

Since V_D is biased at a small value, the above-threshold drain current I_D can then be described by the linear-region current equation [27]

$$I_D = \mu_n C_{\rm ox} \frac{W}{L} \left[(V_{\rm FG} - V_{t0}) V_D - \frac{V_D^2}{2} \right] \tag{8}$$

where μ_n is the electron mobility in the channel of the MOSFET.

Combining (3), (7), and (8), we can further express the channel current I_D as

$$\begin{aligned} I_D = &\mu_n C_{\rm ox} \frac{W}{L} V_D \\ &\cdot \left[\left(\frac{Q + C_{\rm CG} V_{\rm CG0} + C_{\rm CG} V_{\rm CG} \sin \omega t}{C_T} - V_{t0} \right) \right. \\ &\left. + \left(\frac{C_{\rm gd}}{C_T} - \frac{1}{2} \right) V_D \right]. \end{aligned} \tag{9}$$

The slightly increased drain current (see Figs. 8–10) with increasing frequencies has several implications. First, the total net charge Q seen at the FG is increased under the influence of the induced charges at the fluid interface, whose magnitude decreases with the increasing frequency. Second, the change of interface charge may create a fluctuation in the potential ϕ_2 in the liquid bulk [25], causing $C_{\rm SG}$ to decrease with the increasing frequency. This effect results in a smaller C_T, and in turn the increased $C_{\rm CG}/C_T$ ratio contributes more on both the swinging amplitude and the offset voltage, and hence the channel current. The slightly increased drain current implies the charge variation at the solid/liquid interface and thus results in the change of Q or C_T or the combination of both.

At higher frequencies, from 50 kHz to 1 MHz (see Figs. 10–12), the channel current response is getting out of the quasistatic region. Fig. 11 indicates in both water and saturated saline water tests the frequency responses begin to leave the quasistatic region at 100 kHz, yet no major difference is observed between the two. Fig. 12 illustrates eventually the charges seen at the FG fail to respond to the control-gate signal at 1 MHz.

V. Discussion and Conclusion

The modular structure of our CνMOS transistor provides both design convenience and operational functionality for chemical and molecular sensing. The formation of the insulation polymer layer yet needs further attention. With different elastomer mixing ratios, the formed insulation layer will have very different adhesive properties. The polymer layer might either be too hard to carry out the isolation function or too soft to peel off after the pattern transfer. Visual inspection indicates the insulation polymer layer with the reported mixing ratio serves the electrical and physical isolation purposes and is easy to replace or reuse after necessary rinsing and drying steps. For long-term reliability considerations, the insulation scheme can be replaced by a more complex nitride plug design through additional post-processing steps to provide a more robust isolation.

We used polysilicon as the fluid-interaction interface in the conceptual testing stage. Natural silicon oxide grown on the solid/liquid interface will eventually degrade the measurement results and hence influence the reliability. An inert surface coating has to be designed to enhance the stability and reproducibility at the extended floating-gate sensing areas in the long run.

We believe that the incorporation of a multiple-input sensing structure will have the potential to substantially reduce the digital-to-analog conversion and digital signal-processing circuitry, and hence reduce the power consumption normally required for such sensor applications. Also, the EEPROM electron tunneling operations possible with our devices provide additional degree of freedom for the sensing mechanism. Furthermore, the possible array application with various chemoreceptive coatings on different dimensions of SGs will enhance the selectivity of such devices.

The preliminary measurement results suggest the development of the micropower neuromorphic electronic sensing units

TABLE III
ELECTROCHEMICAL MODEL PARAMETERS

Extracted Parameters	C_{CG}	device 1						device 2					
		C_{SG0}	C_{Tc}	C_{Tm}	C_{SG}	C_{difA}	ϕ_2	C_{SG0}	C_{Tc}	C_{Tm}	C_{SG}	C_{difA}	ϕ_2
water	0.4	3.9	1.0	3.9	2.9	**11.8**	**241.6**	18.3	1.5	5.8	4.3	**5.7**	**54.5**
	0.4	3.9	0.9	3.8	2.9	**11.9**	**242.0**	18.3	0.9	5.4	4.5	**5.9**	**56.8**
acetone	0.4	3.9	1.4	3.6	2.2	**4.8**	**320.6**	18.3	1.2	4.4	3.2	**3.9**	**165.6**
	0.4	3.9	1.3	3.6	2.3	**5.5**	**327.1**	18.3	0.9	4.5	3.6	**4.5**	**173.4**

whose structure and function are based on the olfactory and gustatory sensory systems of animals. A complete silicon olfactory and gustatory system including sensing and control units can be expected to be fully integrated on a single chip, and will only dissipate a few hundred microwatts of power in total.

The steady-state and transient models not only provide electrochemical analyzes but also indicate the feasibility of an actuation scheme similar to those used in electrowetting, electroosmotic, and electrophoretic applications. Future efforts will also include the exploration and incorporation of various chemical coatings on the sensing extended floating-gate areas to improve the chemoreceptive selectivity. Further implementation of sensor arrays will also be carried out to establish the lock-and-key mechanism utilizing multiple inputs from the sensing areas.

ACKNOWLEDGMENT

The fabrication of the master silicon substrate was performed at the Cornell Nano-Scale Facility (CNF).

REFERENCES

[1] P. Bergveld, "Development of an ion-sensitive solid-state device for neurophysiological measurements," *IEEE Trans. Biomed. Eng.*, vol. 17, pp. 70–71, Jan. 1970.

[2] W. M. Siu and R. S. C. Cobbold, "Basic properties of the electrolyte-SiO_2-Si system: Physical and theoretical aspects," *IEEE Trans. Electron Devices*, vol. ED-26, pp. 1805–1815, Nov. 1979.

[3] C. Colapicchioni, A. Barbaro, F. Porcelli, and I. Giannini, "Immunoenzymatic assay using CHEMFET devices," *Sens. Actuators B, Chem.*, vol. 4, pp. 245–250, 1991.

[4] M. C. Lonergan, E. J. Severin, B. J. Doleman, S. A. Beaber, R. H. Grubbs, and N. S. Lewis, "Array-based sensing using chemically sensitive, carbon black-polymer resistors," *Chem. Mater.*, vol. 8, pp. 2298–2312, 1996.

[5] F.-P. Steiner, A. Hierlemann, C. Cornila, G. Noetzel, M. Bachtold, J. G. Korvink, W. Gopel, and H. Baltes, "Polymer coated capacitive microintegrated gas sensor," in *Proc. Transducers '95*, 1995, pp. 814–817.

[6] J. van der Spiegel, I. Lauks, P. Chan, and D. Babic, "The extended gate chemically sensitive field effect transistor as multi-species microprobe," *Sens. Actuators*, vol. 4, pp. 291–298, 1983.

[7] R. Smith, R. J. Huber, and J. Janata, "Electrostatically protected ion sensitive field effect transistors," *Sens. Actuators*, vol. 5, no. 2, pp. 127–136, 1984.

[8] L. Bousse, J. Shott, and J. D. Meindl, "A process for the combined fabrication of ion sensors and CMOS circuits," *IEEE Electron Device Lett.*, vol. 9, pp. 44–46, Jan. 1988.

[9] S. W. Wenzel and R. M. White, "A multisensor employing an ultrasonic lamb-wave oscillator," *IEEE Trans. Electron Devices*, vol. 35, pp. 735–743, June 1988.

[10] T. Nakamoto, A. Fukuda, and T. Moriizumi, "Perfume and flavor identification by odor sensing system using quartz-resonator sensor array and neural-network pattern recognition," in *Proc. Transducers '91*, 1991, pp. 355–358.

[11] G. T. A. Kovacs, C. W. Storment, M. Halks-Miller, C. R. Belczynski, C. C. D. Santina, E. R. Lewis, and N. I. Maluf, "Silicon-substrate microelectrode arrays for parallel recording of neural activity in peripheral and cranial nerves," *IEEE Trans. Biomed. Eng.*, vol. 41, pp. 567–577, June 1994.

[12] R. Neuberger, G. Muller, O. Ambacher, and M. Stutzmann, "High-electron-mobility AlGaN/GaN transistors (HEMT's) for fluid monitoring applications," *Phys. Stat. Sol. (a)*, vol. 185, no. 1, pp. 85–89, 2001.

[13] J. Schalwig, G. Muller, O. Ambacher, and M. Stutzmann, "Group-III-nitride based gas sensing devices," *Phys. Stat. Sol. (a)*, vol. 185, no. 1, pp. 39–45, 2001.

[14] H. P. Lang, M. K. Baller, F. M. Battiston, J. Fritz, R. Berger, J. -P. Ramseyer, P. Fornaro, E. Meyer, H. -J. Guntherodt, J. Brugger, U. Drechsler, H. Rothuizen, M. Despont, P. Vettiger, Ch. Gerber, and J. K. Gimzewski, "The nanomechanical NOSE," in *Proc. IEEE MEMS*, 1999, pp. 9–13.

[15] M. J. Madou and S. R. Morrison, *Chemical Sensing with Solid State Devices*. New York: Academic, 1989.

[16] E. Kress-Rogers, *Handbook of Biosensors and Electronic Nose: Medicine, Food, and the Environment*. Boca Raton, FL: CRC Press, 1996.

[17] J. W. Gardner and P. N. Bartlett, *Electronic Noses: Principles and Applications*. London, U.K.: Oxford Univ. Press, 1999.

[18] G. T. A. Kovacs, *Micromachined Transducers Sourcebook*. New York: McGraw-Hill, 1998.

[19] S. D. Senturia, *Microsystem Design*. Norwell, MA: Kluwer, 2000.

[20] A. S. Dewa and W. H. Ko, "Biosensors," in *Semiconductor Sensors*, S. M. Sze, Ed. New York: Wiley, 1994, ch. 9, pp. 425–472.

[21] J. W. Gardner, V. K. Varadan, and O. O. Awadelkarim, *Microsensors, MEMS, and Smart Devices*. New York: Wiley , 2001.

[22] T. Shibata and T. Ohmi, "A functional MOS transistor featuring gate-level weighted sum and threshold operations," *IEEE Trans. Electron Devices*, vol. 39, pp. 1444–1455, June 1992.

[23] J. M. Rabaey, "Designing memory and array structures," in *Digital Integrated Circuits: A Design Perspective*: Prentice Hall, 1996, ch. 10, pp. 551–628.

[24] C. Diorio, P. Hasler, B. A. Minch, and C. A. Mead, "A floating-gate MOS learning array with locally computed weight updates," *IEEE Trans. Electron Devices*, vol. 44, pp. 2281–2289, Dec. 1997.

[25] A. J. Bard and L. R. Faulkner, "Double-layer structure and adsorption," in *Electrochemical Methods: Fundamentals and Applications*. New York: Wiley, 2001, ch. 13, pp. 534–577.

[26] B. A. Minch, "The subthreshold floating-gate MOS transistor," Ph.D. Dissertation, California Institute of Technology, Pasadena, CA, 1997.

[27] R. F. Pierret, *Semiconductor Device Fundamentals*. Reading: Addison-Wesley, MA 1996.

[28] G. Beni and M. A. Tenan, "Dynamics of electrowetting displays," *J. Appl. Phys.*, vol. 52, no. 10, pp. 6011–6015, 1981.

[29] H. Matsumoto and J. E. Colgate, "Preliminary investigation of micropumping based on electrical control of interfacial tension," in *Proc. IEEE MEMS*, 1990, pp. 105–110.

[30] T. Kohashi and T. Kurosawa, "Electroosmotic display device," *IEEE Trans. Electron Devices*, vol. 38, pp. 2064–2069, Sep. 1991.

[31] A. Manz, C. S. Effenhauser, N. Burggraf, D. J. Harrison, K. Seiler, and K. Fluri, "Electroosmotic pumping and electrophoretic separations for miniaturized chemical analysis systems," *J. Micromech. Microeng.*, vol. 4, pp. 257–265, 1994.

[32] R. J. Hunter, *Foundations of Colloid Science*. London, U.K.: Oxford Univ. Press, 2001.

[33] H. Nishiyama and M. Nakamura, "Form and capacitance of parallel-plate capacitors," *IEEE Trans. Comp., Packag., Manufact. Technol. A*, vol. 17, pp. 477–484, 1994.

[34] A. W. Adamson, *Physical Chemistry of Surfaces*. New York: Wiley, 1982.

Nick Yu-Min Shen (S'99) received the B.S. degree in electrical engineering from National Taiwan University, Taipei, Taiwan, R.O.C., in 1995. He began his graduate study in 1998 at the School of Electrical and Computer Engineering, Cornell University, Ithaca, NY, where he is currently pursuing the Ph.D. degree.

In 1995, he served as a Second-Lieutenant Platoon Leader at the National Army Training Center in Tainan, Taiwan, and was promoted to Vice-Commanding Officer in 1997. His research interest is in the development of the micro-scale autonomous system, including electrostatically actuated reconfigurable interconnects, chemoreceptive neuron MOS transistors (CνMOS), the dynamic behavior for MEMS electrostatic devices and the on-chip voltage transformation for MEMS applications.

Zengtao Liu received the B.S. degree in applied physics from Tsinghua University, Beijing, P.R.C. in 1997, and the M.S. and Ph.D. degrees in electrical engineering from Cornell University, Ithaca, NY, in 2000 and 2002, respectively. He was a postdoctoral Associate at the School of Electrical and Computer Engineering, Cornell University, from January to August 2002.

He worked at the Microelectronics division of Lucent Technologies (now Agere systems), Allentown, PA, as an intern during the summer of 2000. His research interest includes nanoscale CMOS, nanocrystal memories, integrated RF systems, and novel MEMS applications for system-on-a-chip. He is now with the nonvolatile memory group of AMD, Inc., Sunnyvale, CA.

Chungho Lee received the B.S. and M.S. degrees in electrical engineering from the University of Seoul, Seoul, Korea, in 1992 and 1994, respectively. He is currently pursuing the Ph.D. degree in electrical engineering at Cornell University, Ithaca, NY.

From 1994 to 2000, he was with Samsung Advanced Institute of Technology, Korea, as a Member of Technical Staff in the material and device sector. His research interests are in the areas of deep submicron CMOS technology and nanocrystal memories.

Bradley A. Minch (S'89–M'97) received the B.S. degree in electrical engineering (with distinction) from Cornell University, Ithaca, NY, in May 1991, and the Ph.D. degree in computation and neural systems from the California Institute of Technology, Pasadena, CA, in June 1997.

He is currently an Assistant Professor in the School of Electrical and Computer Engineering, Cornell University. His research interests include the analog and digital integrated circuit design, translinear circuits, log-domain filters, and adaptive floating-gate MOS circuits.

Dr. Minch received the IEEE Electron Devices Society's Paul Rappaport Award in 1996. Dr. Minch is a member of Tau Beta Pi, Eta Kappa Nu, and Phi Kappa Phi honor societies.

Edwin Chih-Chuan Kan received the B.S. degree from National Taiwan University, Taipei, Taiwan, R.O.C., in 1984, and the M.S. and Ph.D. degrees from University of Illinois, Urbana-Champaign, in 1988 and 1992, respectively.

From January 1992 to 1994 he was with Dawn Technologies as a Principal CAD Engineer of advanced electronic and optical device simulators and technology CAD framework. He was then with Stanford University as a Research Associate from 1994 to 1997, leading projects such as TCAD 1-2-3-D tool development, software architecture definition, model hierarchy and MEMS modeling. From 1997 to 2002, he was an Assistant Professor of the School of Electrical and Computer Engineering, Cornell University, Ithaca, NY, where he is now an Associate Professor. He has spent the summer of 2000 and 2001 at IBM Microelectronics, Yorktown, NY, and at the IBM Faculty Partner program, Fishkill, NY. His main research areas include CMOS technology, semiconductor device physics, system-on-a-chip, composite CAD development, and numerical methods for PDE and ODE.

Dr. Kan received the PECASE (Presidential Early Career Award for Scientists and Engineers) in October 2000 from the White House.